THE JOURNAL OF PHYSICAL CHEMISTRY C

Article

pubs.acs.org/JPCC

Deswelling Mechanisms of Surface-Grafted Poly(NIPAAm) Brush: Molecular Dynamics Simulation Approach

Seung Geol Lee,[†,‡,∥,§] Tod A. Pascal,[‡,∥] Wonsang Koh,[†] Giuseppe F. Brunello,[†] William A. Goddard, III,*[,‡] and Seung Soon Jang*[,†]

[†]Computational NanoBio Technology Laboratory, School of Materials Science and Engineering, Georgia Institute of Technology, 771 Ferst Drive NW, Atlanta, Georgia 30332-0245, United States

[‡]Materials and Process Simulation Center, Division of Chemistry and Chemical Engineering, California Institute of Technology, Pasadena, California 91125, United States

Supporting Information

ABSTRACT: Technologies ranging from solvent extraction and drug delivery to tissue engineering are beginning to benefit from the unique ability of "smart polymers" to undergo controllable structural changes in response to external stimuli. The prototype is poly(*N*-isopropylacrylamide) (P(NIPAAm)) which exhibits an abrupt and reversible hydrophilic to hydrophobic transition above its lower critical solution temperature (LCST) of ∼305 K. We report here molecular dynamics simulations to show the deswelling mechanisms of the hydrated surface-grafted P(NIPAAm) brush at various temperatures such as 275, 290, 320, 345, and 370 K. The deswelling of the P(NIPAAm) brush is clearly observed above the lower critical solution temperature below which the P(NIPAAm) brush is associated with water molecules stably. By simulating the poly(acrylamide) brush as a reference system having the upper critical solution temperature (UCST) behavior with the same conditions employed in the P(NIPAAm) brush simulations, we confirmed that the deswelling of P(NIPAAm) brush does not take place at a given range of temperatures, which validates our simulation procedure. By analyzing the pair correlation functions and the coordination numbers, we found that the dissociation of water from the P(NIPAAm) brush occurs mainly around the isopropyl group of the P(NIPAAm) above the LCST because of its hydrophobicity. We also found that the NH of the amide group in NIPAAm does not actively participate in the hydrogen bonding with water molecules because of the steric hindrance caused by the attached isopropyl group, and thereby the hydrogen bonding interactions between amide groups and water molecules are significantly weakened with increasing temperature, leading to deswelling of the hydrated P(NIPAAm) brush above the LCST through favorable entropic change. These results explain the experimental observations in terms of a simple molecular mechanism for polymer function.

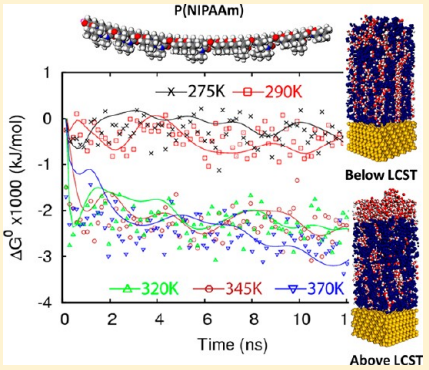

INTRODUCTION

Poly(*N*-isopropylacrylamide), P(NIPAAm), is one of the most widely studied temperature-sensitive polymers. Aqueous solutions of P(NIPAAm) exhibit a lower critical solution temperature (LCST) of approximately 305 K (32 °C) with respect to water,[1,2] meaning that P(NIPAAm) is soluble in water below LCST and becomes less soluble and collapsed to form a separate phase from the water phase above LCST. Due to such characteristics of their phase behavior in water, P(NIPAAm) has been extensively studied for pharmaceutical applications such as drug delivery systems,[3,4] detachment of cultured cells,[5,6] surface-properties control,[7,8] and drug barrier membranes.[9]

To understand the LCST behavior of hydrated P(NIPAAm), several studies have been dedicated to investigate the effect of the presence of polymer chain on the structure and dynamics of water molecules by analyzing the hydrogen bonds the water molecules participate in. Using Raman spectroscopy, Terada and his co-workers found that the polymer chains affect the hydrogen bond of water molecules to cause hydrogen bond defects.[10] Using the same technique, Maeda et al. reported that the number of such hydrogen bond defects in the water phase depends on the hydrophilicity of polymers and the extent of cross-links.[11] The structural change of P(NIPAAm) in water phase was also characterized by Ohta et al. using ^{13}C NMR and ^{1}H NMR, reporting that the isotropic P(NIPAAm) solution was transformed to the gel phase[12] and the mobility of water molecules in the P(NIPAAm) is depressed significantly above LCST.[13] Therefore, it has been clearly confirmed that the P(NIPAAm) solution undergoes serious change in their phase above and below LCST.

On the other hand, a small number of molecular dynamics (MD) simulation studies have also been published to report the changes in the hydrogen bond network and dynamics in water

Received: February 17, 2012
Revised: July 4, 2012
Published: July 11, 2012

phase. Tamai and Tanaka carried out MD simulations for a single P(NIPAAm) chain in the water phase at 200−400 K to study polymer−water and water−water interactions by analyzing the hydrogen bond structure and dynamics[14−16] and reported that the water−water hydrogen bonds are enhanced in the vicinity of polymer segments. Netz and Dorfmüller used the Monte Carlo method to study the diffusion of solute through the gel system[17] and MD simulations to investigate the influence of polymer, especially poly(acryamide) (P(AAm)) on the structure and dynamics of water molecules and hydrogen bonds in the hydrogel system.[18] Simulating cross-linked P(NIPAAm) models at various temperatures, Tonsing et al.[19] found that water molecules can form a hydrogen bond with NH and CO groups in P(NIPAAm) and cross-linkers. Longhi et al.[20] performed MD simulations with 50 units of NIPAAm at 300 and 310 K, from which they reported that the P(NIPAAm) chain equilibrated at 310 K is more compact than that equilibrated at 300 K. Correspondingly, the number of water molecules counted within the first hydration shell at 310 K is smaller by ∼6% than that counted at 300 K. Gangemi et al.[21] also performed MD simulations of a single P(NIPAAm) chain with 3560 water molecules to study the mechanisms of LCST at 302 and 315 K and found that the NIPAAm chain conformation is extended more at 302 K compared to 315 K. Recently, Deshmukh et al.[22,23] investigated the swelling behavior of P(NIPAAm) networks with different cross-linking densities and cross-linkers at 300, 305, and 310 K.

In this study, we are particularly interested in the high-density surface-grafted P(NIPAAm) brush system.[24,25] Since the high-density surface-grafted condition would facilitate the repulsive excluded-volume interaction between brush chains[26] which enables the immediate dehydration and subsequent hydrophobic attraction between the isopropyl groups, it has been known that the high-density surface-grafted P(NIPAAm) brush shows a rapid deswelling behavior above LCST.[27−29] In order to characterize such a rapid temperature responsive molecular system, there have been extensive studies using various analysis techniques such as dynamic light scattering (DLS),[30,31] surface plasmon spectroscopy (SPR),[32] neutron reflectivity (NR),[33−37] quartz crystal microbalance measurement (QCM),[38,39] atomic force microscopy (AFM),[40,41] surface force measurement,[42−44] nuclear magnetic resonance (NMR),[45] and dynamic contact angle measurement.[46,47] It has been also recognized that this high-density surface-grafted P(NIPAAm) can be utilized for numerous developing applications such as aqueous chromatography systems,[48] permeation-controlled porous membranes,[49,50] chemical sensors,[51,52] controlled attachment−detachment surfaces for cultured cells,[53,54] drug release,[55,56] and protein detection,[57,58] evidently showing its promising potential.

In the present study, we perform full-atomistic molecular dynamics (MD) simulations in order to achieve the fundamental understanding of the molecular mechanisms of LCST behavior of the high-density surface grafted P(NIPAAm) brush system, especially focusing on the deswelling process. Through this study, we also expect that the building protocols, the analyzing methodologies, and the understanding of such water−polymer interactions can be extended to other polymeric hydrogels, which will contribute to developing new polymer hydrogels with finely tuned characteristics.

MODELS AND SIMULATIONS DETAILS

Model Constructions. In our simulated models, P(NIPAAm) chains with a degree of polymerization of 30 (Figure 1a) are attached onto the hydrogen terminated silicon

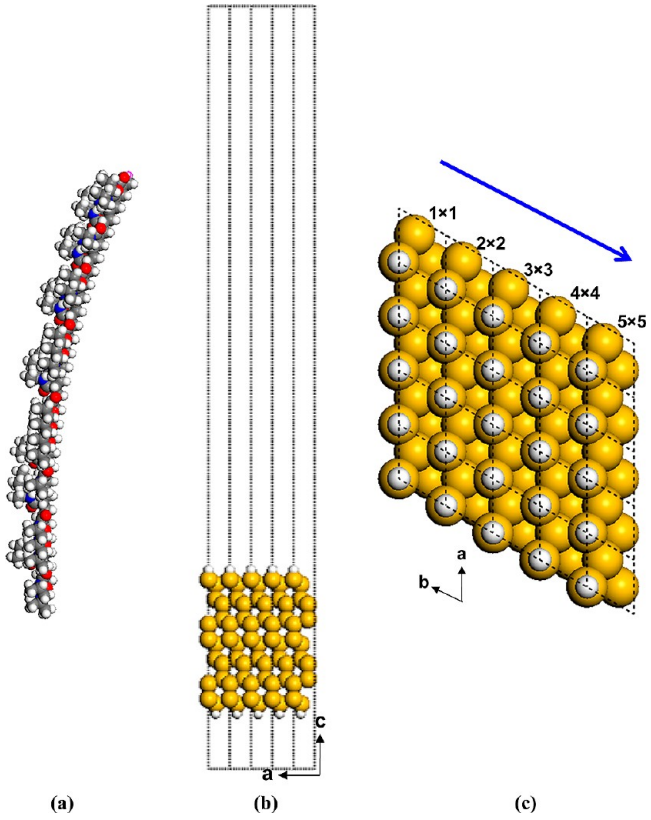

Figure 1. Preparation scheme of the surface-grafted P(NIPAAm) chain on silicon substrate: (a) a single chain of P(NIPAAm) with DP = 30, (b) side view of the silicon substrate, and (c) top view of silicon substrate.

(H−Si) (111) surface by substituting the hydrogen (Figure 1b). In this study, the Si (111) surface was modeled by a slab with the thickness of ∼23 Å. Although the effect of the Si surface is not our interest, the interaction of H−Si (111) surface with P(NIPAAm) chains and water molecules are included in our simulations. To determine probable surface grafting density, we calculated the packing energies by attaching a single P(NIPAAm) chain at various surface areas such as 2 × 2, 3 × 3, 4 × 4, and 5 × 5 surfaces made with the same number of unit surface (1 × 1) as shown in Figure 1c. The packing energy is defined by

$$\Delta E_{\text{packing}} = E_{\text{siliconslab+P(NIPAAm)chain}} - (E_{\text{siliconslab}} + E_{\text{P(NIPAAm)chain}}) \quad (1)$$

where $E_{\text{silicon slab+}P\text{(NIPAAm) chain}}$, $E_{\text{silicon slab}}$, and $E_{\text{P(NIPAAm) chain}}$ denote the energy of the silicon slab with the surface-grafted P(NIPAAm) chain, the energy of the silicon slab, and the energy of the P(NIPAAm) chain, respectively. From Figure 1S (Supporting Information), we found that the 3 × 3 surface (114.93 Å^2/chain) showed the lowest packing energy (∼−17 kcal/mol). Thus, in our study, we use this. Among many factors affecting the phase separation of the polymer brushes, the grafting density plays an important role for the conformational

dx.doi.org/10.1021/jp301610b | J. Phys. Chem. C 2012, 116, 15974−15985

change in the phase separation. Using neutron reflectivity, Yim et al. investigated the conformational changes of P(NIPAAm) chains that were tethered to silicon oxide using a low/high surface grafting density.[33,34] They observed no coil-to-globule transition with a low grafting density ranging from 5000 to 10000 Å^2/chain using molecular weight of 33 000−220 000 Da of P(NIPAAm). To check the effect of the molecular weight on the conformational changes of the brushes for high grafting density (185 Å^2/chain) of P(NIPAAm) chains with three different molecular weights such as 13 000, 44 000, and 71 000 Da, they found a significant conformational transition for all three samples as the temperature passed through LCST, indicating that the high grafting density of the P(NIPAAm) chain is critical for the coil-to-globule transition of the brushes. Plunkett et al. investigated the effect of the grafting density with 303, 476, and 2000 Å^2/chain and the molecular weight of P(NIPAAm) ranged from 51000 to 263 000 Da using surface force measurements.[42] They found that the chain collapse above LCST decreases with decreasing grafting density and molecular weight. Using surface force measurements with grafting densities ranged from 238 to 5000 Å^2/chain, Malham and Bureau reported that the response of the P(NIPAAm) brushes is enhanced with increasing the grafting density of the brushes.[44] Zhu et al. found that the P(NIPAAm) does not collapse above the LCST with very low grafting densities ranged from 3.91×10^8 to 8.33×10^9 Å^2/chain.[43] Using AFM and QCM, Ishida and Biggs investigated the effect of the grafting density using 278, 1429, and 5000 Å^2/chain on the phase separation behavior of P(NIPAAm) brushes.[59] They also reported that the phase separation of P(NIPAAm) brushes depends on the grafting density: the change in the brush layer is more gradual over broad temperature range with increasing the grafting density. LeMieux et al. also showed the clear phase separation of P(NIPAAm) brushes above LCST with a very high grafting density of ∼40 Å^2/chain.[24] In this study, therefore, we think that the grafting density (114.93 Å^2/chain) is high enough to observe the phase separation in comparison with other experimental conditions.[34,42,44,59]

To simulate the surface-grafted P(NIPAAm) brush system using this probable high grafting density, we built an orthorhombic simulation box with lattice parameters of a = 39.91 Å, b = 34.56 Å, and c = 200 Å. as shown in Figure 2a in which the periodic boundary conditions were applied for all three spatial directions. The initial configuration of the twelve surface-grafted P(NIPAAm) chains within the orthorhombic simulation box are also shown in Figure 2b. To add water molecules into the P(NIPAAm) brush system, we used Monte Carlo techniques to add 1300 water molecules into the brush (Figure 2c with the reduced van der Waals parameter (30% of original value), which corresponds to the water content of ∼40 wt %. After adding water molecules, the energy minimization was performed with the original van der Waals parameters to adjust the positions of water molecules.

Model Equilibration. After this initial structure was prepared, we equilibrated the system by performing NVT MD simulations at 290 K for 20 ns. After this equilibration, we independently simulated the model system at five different temperature conditions such as 275, 290, 320, 345 and 370 K. Because the aqueous solutions of P(NIPAAm) exhibit the LCST at ∼305 K (32 °C),[1,2,60,61] two temperature conditions (275 and 290 K) are below the LCST and three temperature conditions (320, 345, and 370 K) are above the LCST. We completed another 10 or 15 ns of MD simulations for

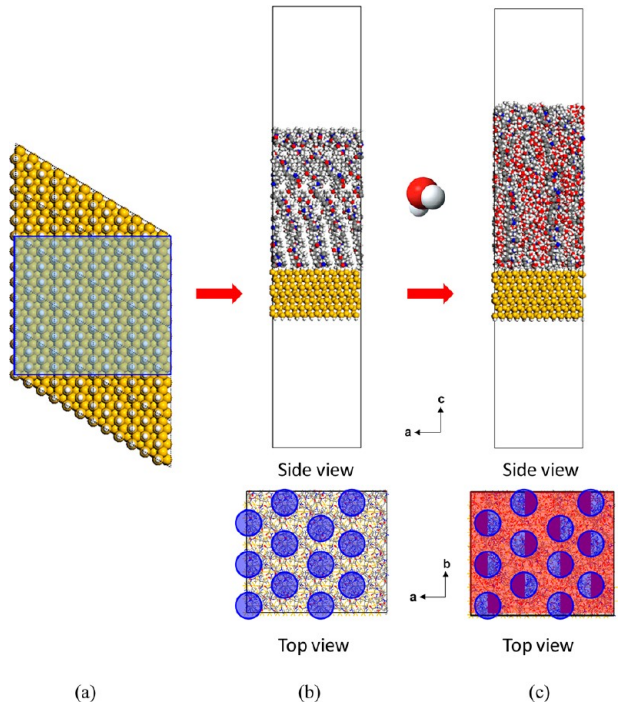

Figure 2. Preparation of the initial configurations of the surface-grafted P(NIPAAm) brushes on the silicon slab: (a) a hexagonal closed packing mode is retained in an orthorhombic simulation box (blue box) with the lattice parameters of a = 39.91 Å, b = 34.56 Å, and c = 200 Å; (b) the initial configuration of the surface-grafted P(NIPAAm) brushes, consisting of 12 P(NIPAAm) chains, with blue circles indicating the location of each brush in the system; and (c) hydrated P(NIPAAm) brushes with 1300 water molecules, with blue circles and red color indicating the location of each brush and water molecules in the system, respectively.

temperatures below LCST and above LCST, respectively, to monitor the temperature-dependent volumetric change of the P(NIPAAm) brushes until the system was equilibrated.

Force Field and MD Parameters. In this investigation, we employed the generic DREIDING force field,[62] which has been well tested in various organic systems such as polymer electrolyte membranes,[63−69] the self-assemblies of organic molecules,[70−72] and hydrogels.[73−77] The F3C force field[78] was also used to describe water molecules in the hydrogel systems. Although various water models such as SPC and TIP3P can also produce high quality simulations for water and hydrated macromolecules, we think that the fully flexible nature of F3C is the undeniable advantage because the F3C water model is easily integrated and simulated with any full-atomistic models in classical MD simulations. Indeed, we have used the F3C water model successfully in various studies above-mentioned.[63−77] Thus, the total potential energy is given as follows:

$$E_{\text{total}} = E_{\text{vdW}} + E_{\text{electostatic}} + E_{\text{bond}} + E_{\text{angle}} + E_{\text{torsion}} + E_{\text{inversion}} \quad (2)$$

where E_{total}, E_{vdW}, $E_{\text{electrostatic}}$, E_{bond}, E_{angle}, E_{torsion}, and $E_{\text{inversion}}$ are the energies for the total, van der Waals, electrostatic, bond stretching, angle bending, torsion, and inversion components, respectively. The details of the force field parameters have already been described.[62,78] For MD simulations, the velocity-Verlet algorithm[79] method was used to integrate the equations

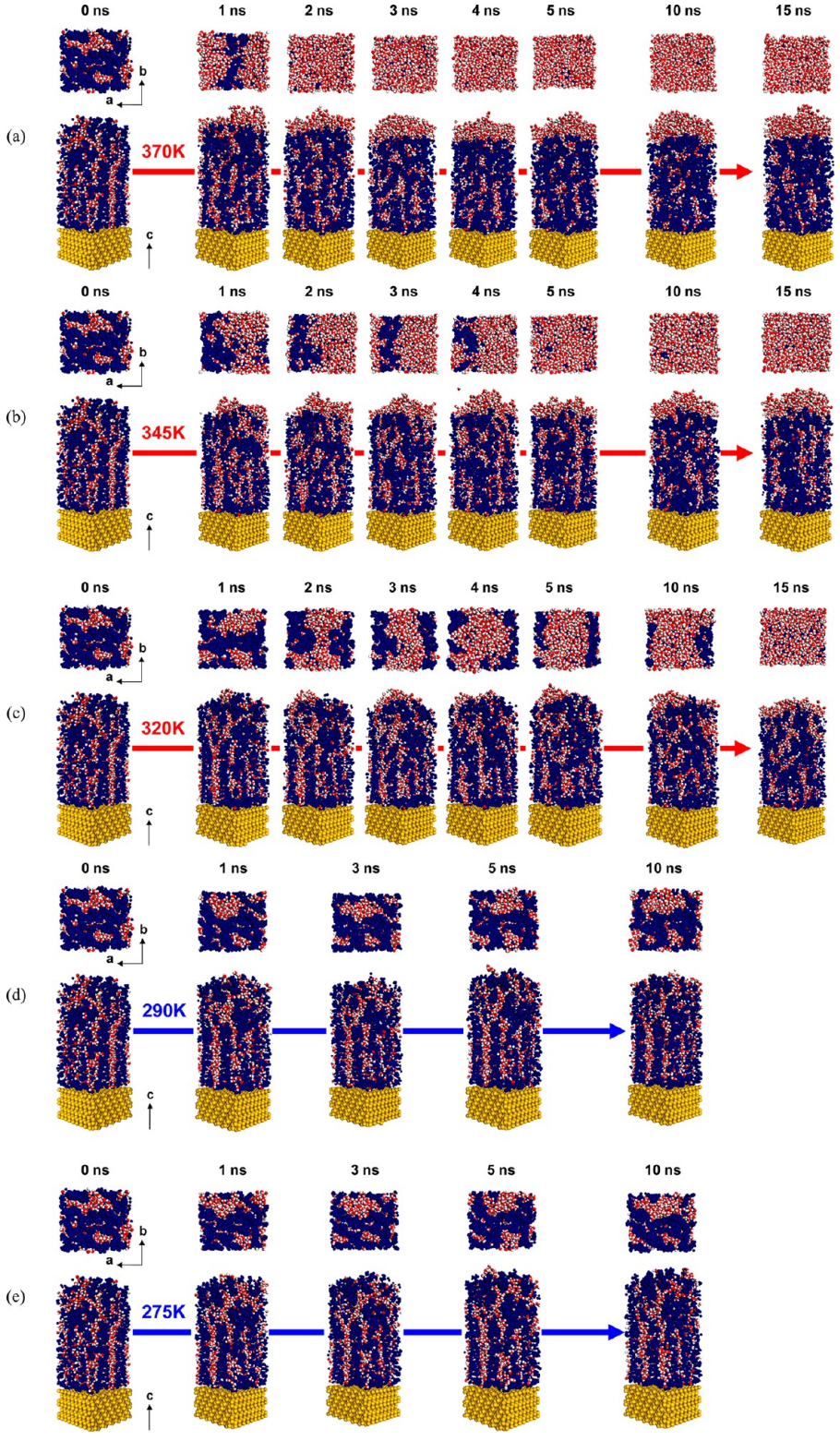

Figure 3. Snapshots of the hydrated surface-grafted P(NIPAAm) brushes during the MD simulation at (a) 370, (b) 345, (c) 320, (d) 290, and (e) 275 K. Blue, yellow, red, and white color denote polymer brushes, silicon substrate, oxygen of water, and hydrogen of water, respectively.

of motion with a time step of 1.0 fs. A Nose-Hoover thermostat[80−82] was used with a damping relaxation time of 0.1 ps and a dimensionless cell mass factor of 1.0, respectively. During simulation, all of the valence parameters were fully unconstrained. The time interval between samplings was 5 ps. The atomic charges of the polymers were assigned using Mulliken population analysis[83] at the level of B3LYP/6-31G** (Jaguar quantum chemistry software)[84] and the atomic charges of water molecules were the outputs of the F3C water model.[78] The Lennard-Jones (LJ) potential was smoothly shifted to zero between 1.2 and 1.5 nm. A particle−particle particle−mesh (PPPM) method[85] is used to calculate the electrostatic

dx.doi.org/10.1021/jp301610b | J. Phys. Chem. C 2012, 116, 15974−15985

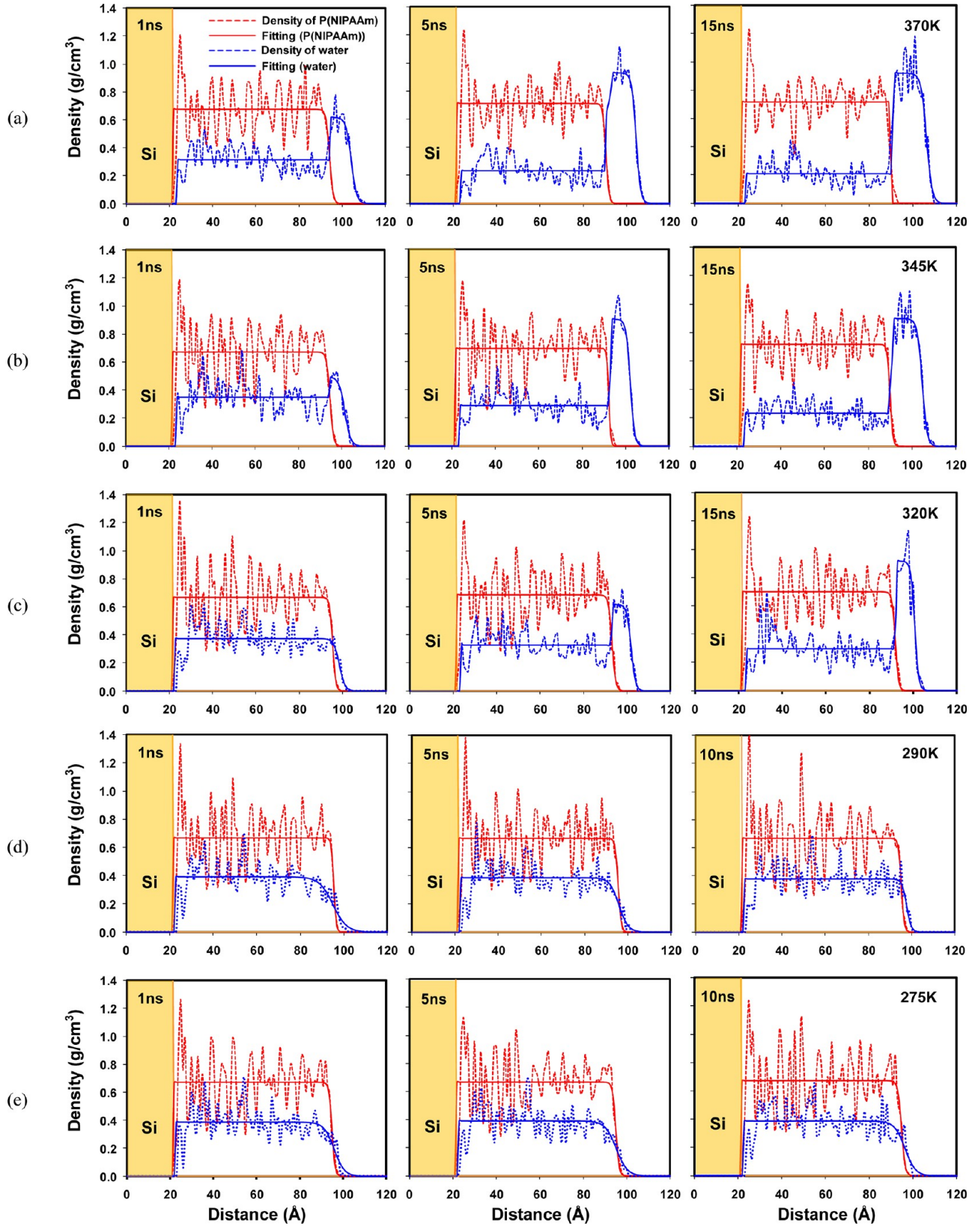

Figure 4. Density profiles of the surface-grafted P(NIPAAm) brushes at (a) 370, (b) 345, (c) 320, (d) 295, and (e) 275 K.

interactions. The MD simulation code used in this study is the large-scale atomic/molecular massively parallel simulator (LAMMPS) MD simulator that was developed by Plimpton at Sandia National Laboratories.[86,87]

Thermodynamic Properties. We calculated the absolute entropy and quantum corrections to the energy (zero-point energy and heat capacity) every 100 ps along the 15 ns MD simulation using the two-phase thermodynamics (2PT)

dx.doi.org/10.1021/jp301610b | J. Phys. Chem. C 2012, 116, 15974−15985

method.[88,89] Here, the atomic velocities and coordinates were recorded every 4 fs during a 20 ps NVT MD simulation, since the method relies on accurate sampling of the fastest vibrational modes, which have periods of ~10 fs for a 3000 cm^{-1} vibration. Lin, Blanco, and Goddard[89] (LBG) showed that that a 20 ps trajectory is sufficient to obtain an accurate entropy of a Lennard-Jones fluid and liquid water.[88] In addition the 2PT model has been successful in calculating the entropy of water in different domains of PAMAM dendrimers,[90] in determining various phases of dendrimer liquid crystals,[91] and in calculating the relative stability of various aggregates.[92] Jana et al.[93] used 2PT to show that water molecules in both grooves of DNA, have significantly lower entropies than for bulk water. Pascal et al showed that 2PT is capable of accurately predicting the thermodynamics of a hydrogel with varying water content[94] and in capturing the thermodynamics of water under confinement in nanotubes.[95]

RESULTS AND DISCUSSION

Density Profiles. The snapshots of the surface-grafted P(NIPAAm) brushes during MD simulation (Figure 3) show that the P(NIPAAm) brushes are deswelled above LCST (~305 K) of P(NIPAAm), as shown in Figure 3a–c. We observed faster deswelling at higher temperatures. However, we did not observe the deswelling of water molecules below the LCST, as shown in Figure 3, d and e.

We analyzed the snapshots to provide the distributions of each component throughout the hydrated brushes using density profiles along the *c*-axis direction of the simulation box (Figure 4) at each temperature: water molecules (blue line), polymer brushes (red line) and silicon substrate (orange color). The density profiles from 370 (Figure 4a), 345 (Figure 4b), and 320 K (Figure 4c) show the development of a dissociated water slab above 90 Å from the Si (111) surface. Again, we did not observe any water slab out of the brushes below the LCST, as shown in Figure 4d (290 K) and Figure 4e (275 K).

To quantify the change in the thickness of the brushes, we define the "90-interface" of the polymer brushes along the *c*-axis direction where the density of the brushes is 90% of its maximum value. In the same manner, we also define the "90-interface" of the water slab at the water-vacuum interface where the density of the water slab is 90% of its maximum value. Therefore, the thickness of the water slab is defined by the distance between two points, the "90-interface" of the polymer brushes and the "90-interface" of the water slab (Figure 5). As the simulation proceeds, the thickness of the water slab out of the brushes (Figure 6a) and the number of water molecules increase (Figure 6b) above the LCST. Percentages of 30%, 46%, and 52% of the total water molecules were squeezed out of the brushes at 320, 345, and 370 K during 15 ns MD simulations, respectively. The density of the water slab out of the brushes (Figure 6c) is increased, while the density of the water in the brushes (Figure 6d) is decreased above the LCST. The density of the water slab out of the brushes reaches the maximum value at 15 (320 K), 5 (345 K), and 2 ns (370 K), meaning that the deswelling process is accelerated with increasing temperature. In contrast, we did not observe any significant changes in the density profiles below LCST during the simulations. The thickness of the brushes (Figure 6e) decreases and correspondingly, the density of the brushes (Figure 6f) increases, indicating the deswelling of the brush above LCST.

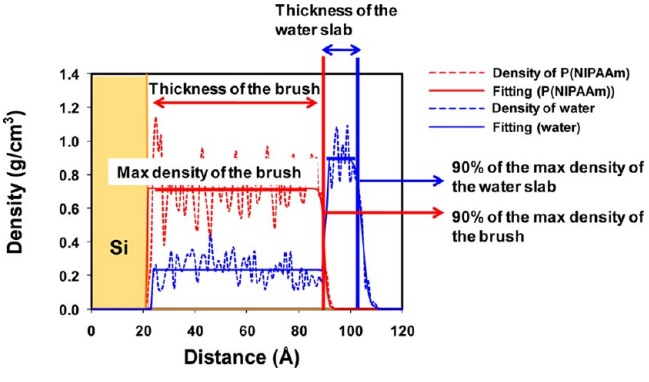

Figure 5. Scheme to determine the thickness of the brushes and the water slab.

We also prepared a reference system to compare/validate the results of the simulations in this study. The reference system consists of surface-grafted poly(acrylamide) (P(AAm)) brush instead of P(NIPAAm). The other conditions for MD simulations are the same as the P(NIPAAm) brush systems. Although P(AAm) has a similar chemical structure to P(NIPAAm), P(AAm) does not contain the hydrophobic isopropyl group. Correspondingly, P(AAm) shows an upper critical solution temperature (UCST) with respect to water at 235 K,[96] and therefore, P(AAm) does not show phase separation behavior with liquid water. We expect that the P(AAm) brush will not go through the deswelling in the range of the simulated temperatures for the P(NIPAAm) brush. To check this expectation, we simulated the surface-grafted P(AAm) brush with 1300 water molecules (~50 wt % water content) at 275, 290, 320, 345, and 370 K. Since we observed the rapid deswelling within 5 ns for the P(NIPAAm) brushes (Figure 6b), we performed MD simulations of the P(AAm) brushes for 5 ns for comparison. From the snapshots (Figure 2S, Supporting Information) and the density profiles (Figure 3S, Supporting Information), the P(AAm) brush system did not show the deswelling process or the development of a water slab, even with a higher water content (~50 wt %) compared to that of the P(NIPAAm) brush (~40 wt %). The thickness of the P(AAm) brush (Figure 4S, Supporting Information) increases with increasing temperature due to thermal expansion. The change in thickness of the P(AAm) brush as a function of temperature occurs in the opposite direction to that of the P(NIPAAm) brush as shown in Figure 6e.

Inner Structures of Surface-Grafted Brush in the Presence of Water Molecules. To investigate the inner structures of the surface-grafted brushes with the water molecules, we analyzed the pair correlation function (PCF) of the following pairs:

(i) The oxygen (NIPAAm)–oxygen (water) pair ($\rho g_{O(NIPAAm)-O(water)}$); the oxygen (AAm)–oxygen (water) pair ($\rho g_{O(AAm)-O(water)}$);
(ii) The nitrogen (NIPAAm)–oxygen (water) pair ($\rho g_{N(NIPAAm)-O(water)}$); the nitrogen (AAm)–oxygen (water) pair ($\rho g_{N(AAm)-O(water)}$);
(iii) The methyl carbon (NIPAAm)–oxygen (water) pair ($\rho g_{C(NIPAAm)-O(water)}$).

The atoms used for this PCF analysis are shown in Figure 7. The PCF, $g_{A-B}(r)$ is the probability density of finding atoms A and B at a distance r averaged over the equilibrium trajectory, which is defined by

dx.doi.org/10.1021/jp301610b | J. Phys. Chem. C 2012, 116, 15974–15985

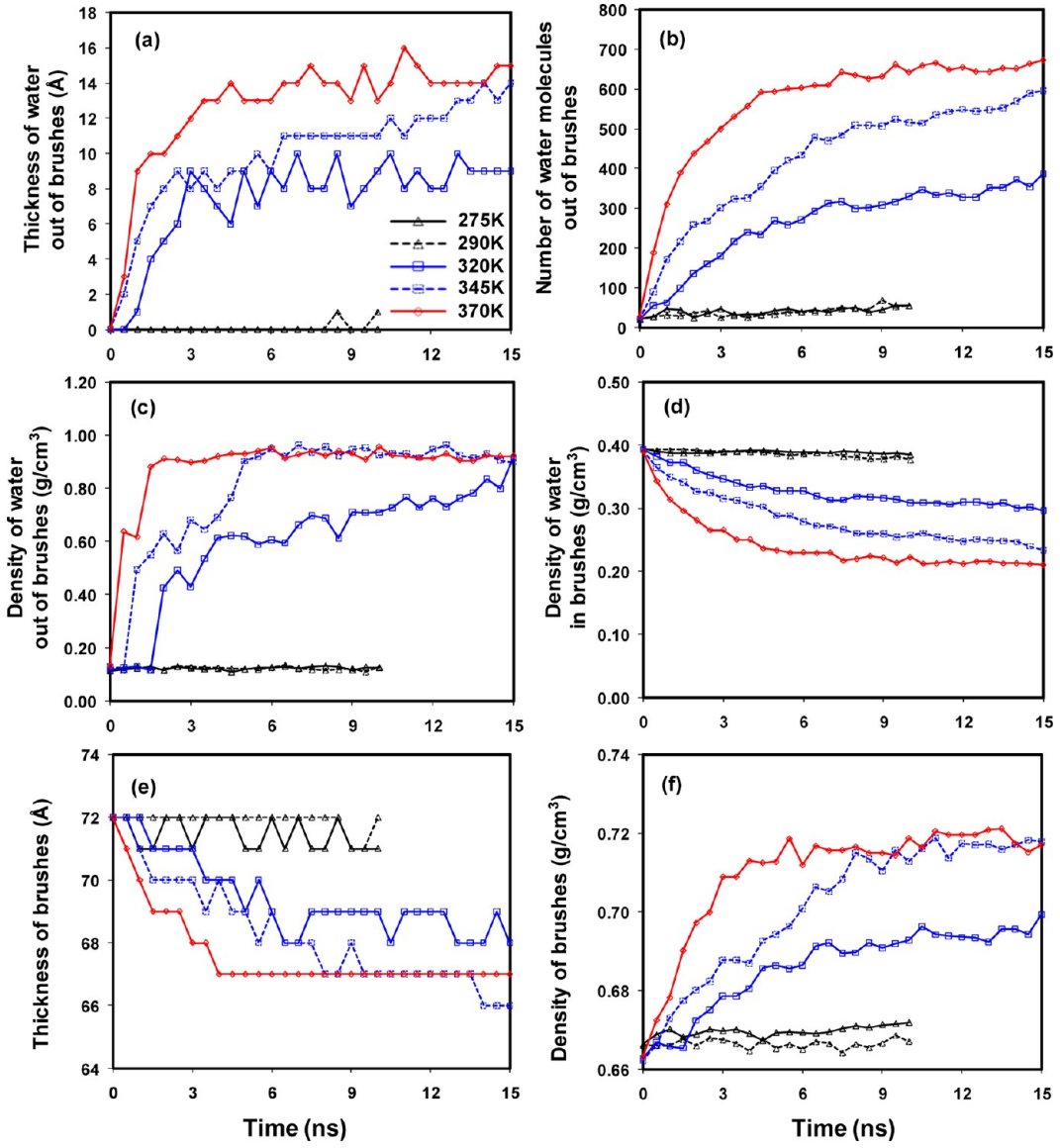

Figure 6. (a) Thickness of the water out of the P(NIPAAm) brushes, (b) number of water molecules out of the P(NIPAAm) brushes, (c) density of the water out of the P(NIPAAm) brushes, (d) density of the water in the P(NIPAAm) brushes; (e) thickness of the P(NIPAAm) brushes, and (f) density of the P(NIPAAm) brushes.

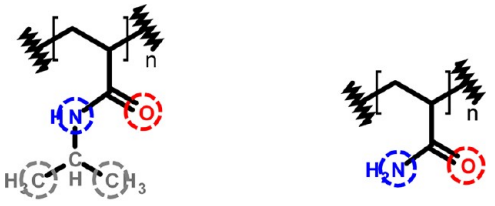

(a) (b)

Figure 7. Atoms used to calculate the pair correlation function: (a) P(NIPAAm) and (b) P(AAm).

$$g_{A-B}(r) = \left(\frac{n_B}{4\pi r^2 dr}\right) / \left(\frac{N_B}{V}\right) \quad (3)$$

where n_B is the number of particle B located at a distance r in a shell of thickness dr from particle A, N_B is the number of B particles in the system, and V is the total volume of the system. Using this pair correlation function, we can analyze the environment the water molecules are located in.

First, $\rho g_{O(NIPAAm)-O(water)}$ in Figure 8a shows that the intensity of the peak decreases as a function of simulation time above LCST while the intensity the peak does not change during the simulation below LCST. This is clearly due to the deswelling of the P(NIPAAm) brush. On the contrary, $\rho g_{O(AAm)-O(water)}$ (Figure 5Sa, Supporting Information) remains nearly the same during the simulation. $\rho g_{N(NIPAAm)-O(water)}$ in Figure 8b also decreases above LCST while it does not change below LCST. Similarly, such LCST behavior is observed in the methyl carbon of the isopropyl group in P(NIPAAm) brush ($\rho g_{C(NIPAAm)-O(water)}$) as shown in Figure 8c.

To quantify the change in the PCFs, we calculated the coordination number (CN) by integrating the first solvation shell as shown in Figure 9. First, it is observed that the water CNs for the nitrogen ($N_{(NIPAAm)}$), the carbonyl oxygen ($O_{(NIPAAm)}$) and the methyl carbon ($C_{(NIPAAm)}$) have different values: the hydrophobic $C_{(NIPAAm)}$ and the $O_{(NIPAAm)}$) have the

dx.doi.org/10.1021/jp301610b | J. Phys. Chem. C 2012, 116, 15974−15985

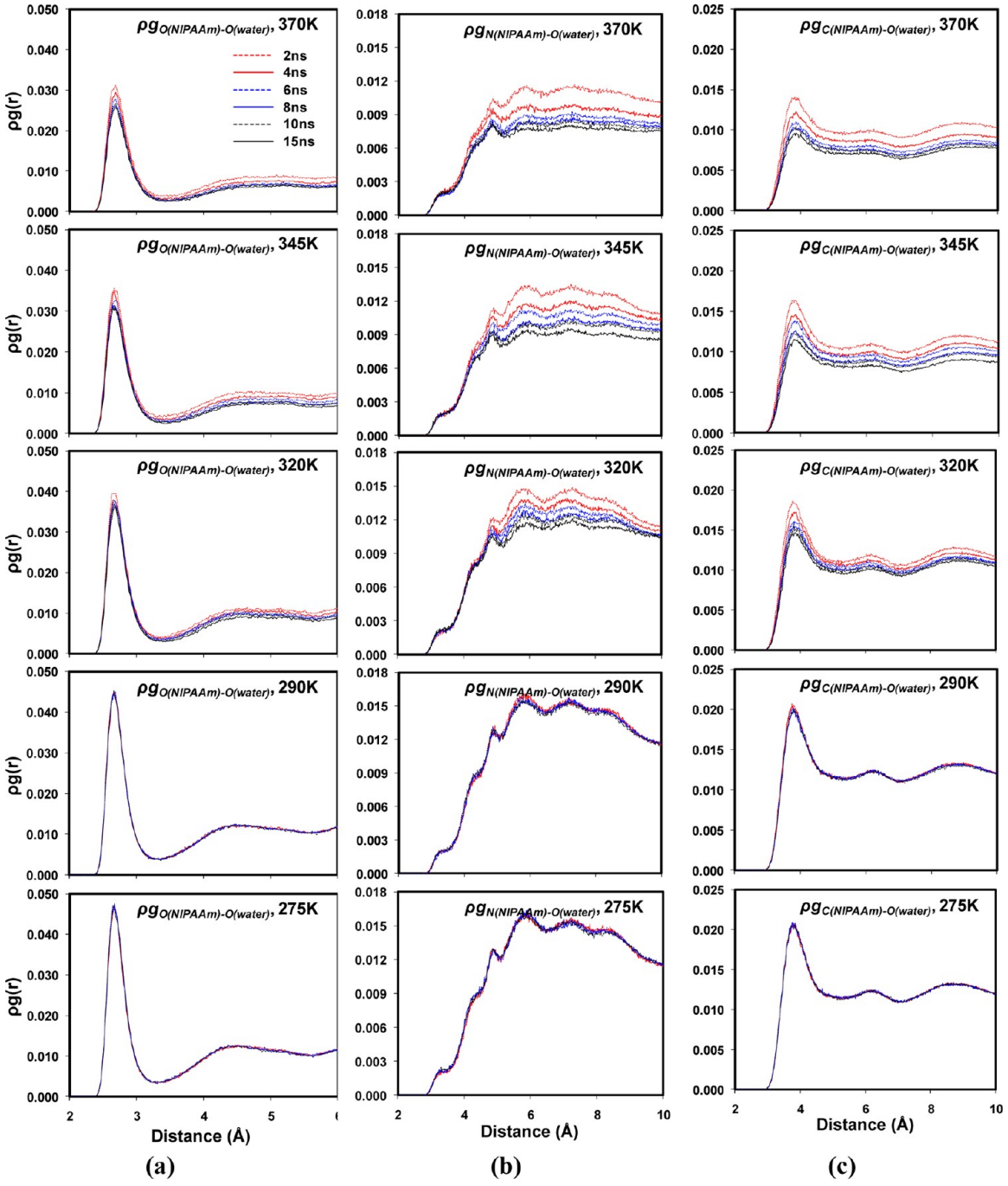

Figure 8. Pair correlation functions of (a) O(NIPAAm)−O(water) pairs, (b) N(NIPAAm)−O(water) pairs, and (c) C(NIPAAm)−O(water) pairs.

largest and the second largest CN values, respectively, whereas the CN for the $N_{(NIPAAm)}$ has the smallest value close zero. Considering the chemical structure of P(NIPAAm) in Figure 7, the result in Figure 9 indicates that the water CNs are dependent on the exposure of each atom to water molecules. In other words, although the $C_{(NIPAAm)}$ is in the hydrophobic isopropyl moiety, it is well exposed to water molecules as the terminal group of the side chain, and thereby has the largest water CN value. Thus, the smallest water CN for $N_{(NIPAAm)}$ is due to the steric hindrance from the isopropyl group.

On the other hand, Figure 9a shows that above LCST, the water CN of $C_{(NIPAAm)}$ decreases more rapidly than that of the $O_{(NIPAAm)}$. This change of the water CN is expressed as $\Delta CN = CN_f - CN_i$ where CN_i and CN_f are the initial and the final value of CN from the MD trajectories, respectively, as summarized in Table 1. It is found that ΔCN for the $C_{(NIPAAm)}$ is changed from −0.88 to −1.36 with increasing temperature above LCST more significantly than that for the rest (fomr 0.02 to 0.00 for the $N_{(NIPAAm)}$; from −0.21 to −0.38 for the $O_{(NIPAAm)}$). We think this is because the $C_{(NIPAAm)}$ does not offer sufficient interaction with water molecules and thereby, the deswelling starts distinctly around the isopropyl group of the P(NIPAAm) brush above LCST. In contrast, for the polymer−polymer pair, we observed that the CN for the $O_{(NIPAAm)}$−$O_{(NIPAAm)}$ pair (Figure 9b) and $N_{(NIPAAm)}$−$N_{(NIPAAm)}$ pair (Figure 9c) pair increase with increasing temperature above LCST.

dx.doi.org/10.1021/jp301610b | J. Phys. Chem. C 2012, 116, 15974−15985

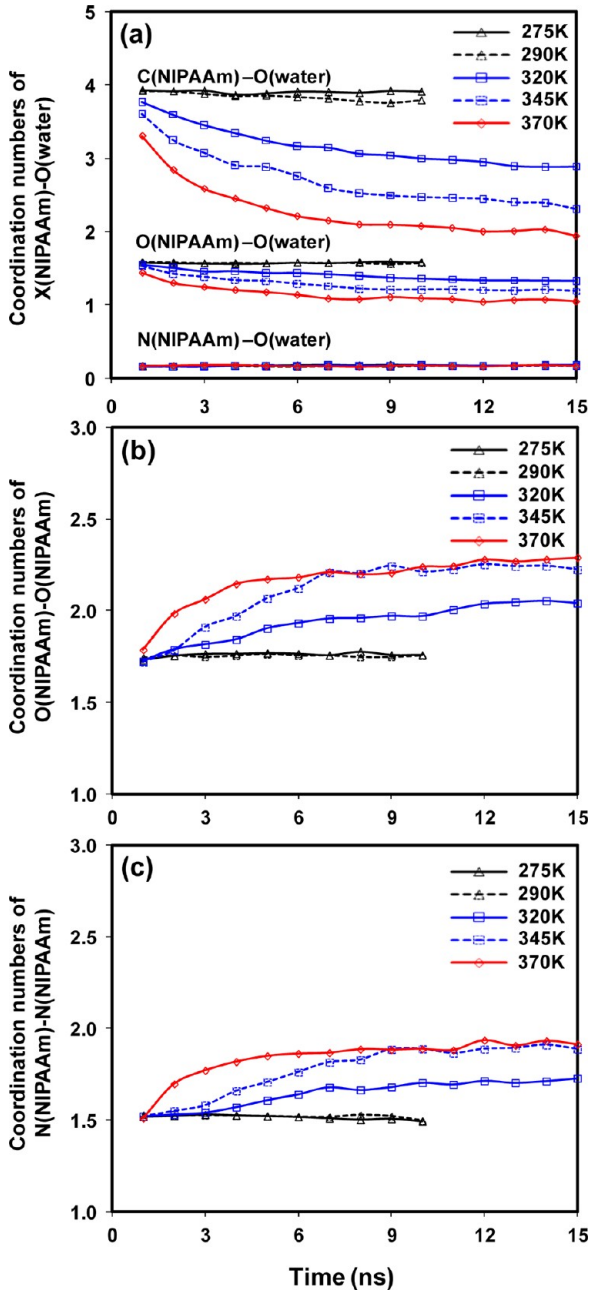

Figure 9. Change in the coordination numbers for (a) X(NIPAAm)–O(water) X = C, O or N, (b) O(NIPAAm)–O(NIPAAm), and (c) N(NIPAAm)–N(NIPAAm).

We also calculated the CNs for the $N_{(AAm)}$ and the $O_{(AAm)}$ (Table 1) in order to compare the temperature-dependent phase behavior of P(NIPAAm) brush and P(AAm) brush. The $N_{(AAm)}$ has now even larger CN value in comparison with the $O_{(AAm)}$ because there is no blocking isopropyl group. Another point we stress here is that there is no significant reduction of the CN value above 320 K above which the P(NIPAAm) brush undergoes deswelling, clearly demonstrating that the P(AAm) brush has the UCST behavior.

Hydrogen Bonding Analysis. Since hydrogen bond has been noticed to play an important role in the LCST behavior,[29,97,98] we monitored the change in the hydrogen bonds between polar groups and water molecules using the geometric criteria suggested by Chandler.[99] According to

Table 1. Water Coordination Numbers for P(NIPAAm) and P(AAm)

		CN			
atoms	temp (K)	initial value CN_i	final value CN_f	$\Delta CN = CN_f - CN_i$	range of distance, r (Å)
O_{NIPAAm}	370	1.43	1.05	−0.38	<3.4
	345	1.52	1.18	−0.34	
	320	1.54	1.33	−0.21	
	290	1.59	1.56	−0.03	
	275	1.58	1.58	0.00	
N_{NIPAAm}	370	0.16	0.16	0.00	<3.6
	345	0.16	0.16	0.00	
	320	0.16	0.18	0.02	
	290	0.16	0.17	0.01	
	275	0.16	0.18	0.02	
C_{NIPAAm}	370	3.30	1.94	−1.36	<4.5
	345	3.60	2.31	−1.29	
	320	3.77	2.89	−0.88	
	290	3.92	3.79	−0.13	
	275	3.93	3.91	−0.02	
O_{AAm}	370	1.68	1.67	−0.01	<3.4
	345	1.71	1.67	−0.04	
	320	1.76	1.78	0.02	
	290	1.82	1.78	−0.04	
	275	1.77	1.78	0.01	
N_{AAm}	370	2.00	1.97	−0.03	<3.6
	345	2.08	2.05	−0.03	
	320	2.20	2.27	0.07	
	290	2.28	2.31	0.03	
	275	2.33	2.35	0.02	

Chandler, a hydrogen bond is formed between a pair of molecules if the distances and angle satisfy the following conditions:

$$R_{OO} \leq 3.60 \text{ Å}$$
$$R_{OH} \leq 2.45 \text{ Å}$$
$$\Phi \leq 30^\circ \quad (4)$$

where R_{OO} and R_{OH} are the intermolecular oxygen–oxygen distance ($O_1 \cdots O_2$) and the intermolecular oxygen–hydrogen distance ($O_1 \cdots H_2$), respectively, and Φ is an angle of $O_1 \cdots O_2$–H_2.

Figure 10 shows the change in the total number of hydrogen bonds between the polar groups (=O and –NH of P(NIPAAm)) and the water molecules. The number of hydrogen bonds for the $O_{(NIPAAm)}$–water pairs is changed from 419 (at the initial time frame) to 330 (at the final time frame) for 370 K, from 469 to 388 for 345 K, from 496 to 421 for 320 K, from 501 to 505 for 290 K, and from 503 to 504 for 275 K, meaning that above LCST the hydrogen bonds between the P(NIPAAm) brush and the water molecules are reduced with increasing temperature, which leads to the deswelling of the P(NIPAAm) brush, whereas below LCST, the number of the hydrogen bonds remains nearly the same. The contribution of the $NH_{(NIPAAm)}$–water pairs is also insignificant since the number of hydrogen bonds is ~20, indicating that the hydrogen bond interaction between the NH group and the water molecules is not developed well due to the steric hindrances from the isopropyl group. These results agree well with those of the PCFs and CNs. In contrast, it is observed that the hydrogen

dx.doi.org/10.1021/jp301610b | J. Phys. Chem. C 2012, 116, 15974–15985

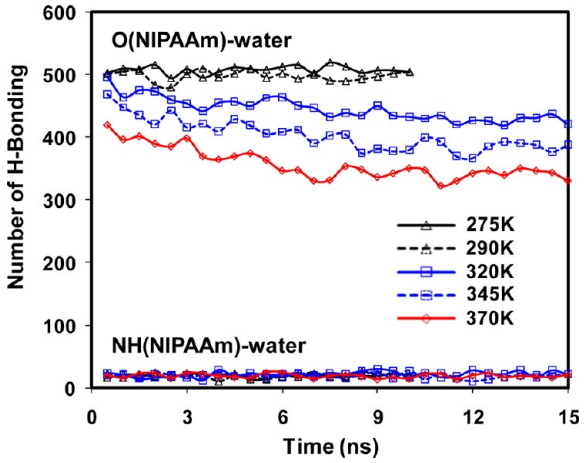

Figure 10. Total number of hydrogen bonds in P(NIPAAm) brushes.

bonds between the P(AAm) and water molecules behaves differently as presented in Figure 7S (Supporting Information). The hydrogen bond for $NH_{2(AAm)}$ shows no temperature dependency, indicating that the water molecules stay within P(AAm) brush well above 320 K, whereas $O_{(AAm)}$ also accommodates ~90% of water molecules stably during the simulations. We believe that this difference is due to the hydrophilicity of polymer greatly enhanced by removing the hydrophobic isopropyl group in P(NIPAAm).

Total Surface Area of the Surface-Grafted Brush. Above LCST, it is expected that the total surface area of the P(NIPAAm) brush will be decreased due to its deswelling and collapse, through which the water accessibility to the brush will be reduced. To analyze this, we monitored the change in the total surface area of the P(NIPAAm) and P(AAm) brushes which is accessible to the water molecules (solvent) as shown in Figure 11 and Figure 8S (Supporting Information), respectively. This solvent accessible surface area (SASA) is calculated by rolling the probe over the van der Waals surface of the solute. The radius of the probe is 1.4 Å corresponding to water molecule. From Figure 11, it is clear that the total surface area of the P(NIPAAm) brush is decreased above LCST, and its extent of the decrease is more significant with increasing temperature, whereas the P(AAm) brush does not have such decrease over the range of simulation temperature.

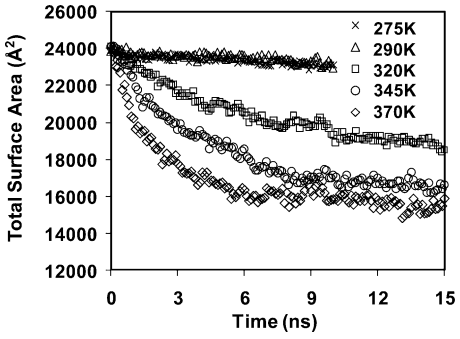

Figure 11. Total surface area of P(NIPAAm) brush system.

Thermodynamic Properties. In this study, we monitored the change of the Gibbs free energy as a function of simulation time using the 2PT method.[88,89] In Figure 12a, it is clear that the Gibbs free energy is decreased above LCST (at 320, 345, and 370 K) and converges between 6 and 8 ns of dynamics.

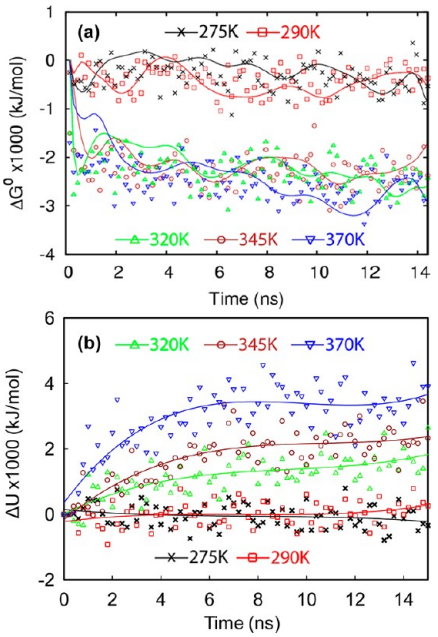

Figure 12. (a) Gibbs free energy of hydrated P(NIPAAm) brush during 15 ns NVT-MD simulation. The free energies are calculated every 100 ps using the 2PT method. The actual free energies (symbols) are smoothed with a cubic Bezier function (solid lines) for presentation purposes. The free energy at 275 (black ×) and 290 K (red squares) are relatively unchanged on the time scale of our simulations, whereas a dramatic decrease is observed at 320 (green upward triangles), 345 (brown circles), and 370 K (blue downward triangles). (b) Potential energy of hydrated P(NIPAAm) brush during 15 ns NVT-MD simulation.

This is in general agreement with the time scale of the polymer–water separation observed previously. Below LCST (at 290 and 275 K), we do not observe significant changes in the free energy of the system: there is an initial decrease as the system achieves thermodynamic equilibrium and the free energy oscillates close to the average during the entire dynamics. Through this analysis, therefore, it is found that this deswelling of P(NIPAAm) brush above LCST is thermodynamically driven to reduce its Gibbs free energy by increasing entropy. This is clear from Figure 12b presenting that the potential energy becomes unstable above LCST. In other words, the phase separation develops even though the potential energy increases, which is due to the increase of entropy. Obviously, the increased temperature signifies the entropic contribution of the water molecules in the P(NIPAAm) brush, causing them to separate and form water phase at the top of the polymer.

■ CONCLUSIONS

In this study, we investigated the mechanism of the LCST behavior of hydrated P(NIPAAm) brush using full-atomistic MD simulations at a high grafting density condition (114.93 Å^2/chain). First, by analyzing the density profiles as the simulation proceeds, we observed that, at the temperatures above LCST (~305 K) such as 320, 245, and 370 K, the water molecules were dissociated from the brush to form separated water phase, and simultaneously, the brush was collapsed, which was not observed at the temperatures below LCST such as 275 and 290 K. From the results that the deswelling process was accelerated with increasing temperature, implying that such

dx.doi.org/10.1021/jp301610b | J. Phys. Chem. C 2012, 116, 15974–15985

deswelling is driven by the entropy rather than energy. We also simulated the hydrated P(AAm) brush with the same packing condition with the P(NIPAAm) brush for comparison of the water-polymer interaction. It was confirmed that the hydrated P(AAm) brush does not undergo the deswelling process although it has even higher water content (~50 wt %) than the P(NIPAAm) brush has (~40 w %). Considering the fact that the P(AAm) has UCST (~235 K)[96] in reality, such different deswelling process of P(NIPAAm) from that of P(AAm) in the in our simulations validates the soundness of the simulation methods we employed. Second, through the pair correlation function analysis, we found that the P(NIPAAm) side chains were dissociated from the water molecules, especially the two hydrophobic methyl ($-CH_3$) groups underwent the most serious reduction of the interaction with water molecules. On the contrary, the P(AAm) brush did not show any significant reduction of the interaction with water molecules over the range of the simulated temperature. From these results, we infer that the isopropyl group attached to amide moiety deprives the amide moiety of its capability to form the hydrogen bond with water molecules. The collapse of the P(NIPAAm) brush was also confirmed through the water accessible surface area analysis as well as the density profile analysis, showing that the volume occupied by water disappears as the water molecules are squeezed out of the brush.

Finally, the thermodynamic driving force was evaluated by calculating the Gibb free energy as well as energy using the 2PT method. It was observed that, above LCST, the Gibbs free energy (ΔG) is reduced although the energy (ΔU) is increased, whereas below LCST, the ΔG and ΔU remain nearly the same. Therefore, we found that the LCST of the P(NIPAAm) brush is driven by the entropic contribution.

■ ASSOCIATED CONTENT

Supporting Information

Additional figures of experimental data (Figures 1S–7S). This material is available free of charge via the Internet at http://pubs.acs.org.

■ AUTHOR INFORMATION

Corresponding Author

*E-mail: SeungSoon.Jang@mse.gatech.edu (S.S.J.); wag@wag.caltech.edu (W.A.G.).

Present Address

[§]Agency for Defense Development, Yuseong P.O. Box 35, Daejeon, 305-600 South Korea.

Author Contributions

[∥]These authors contributed equally to this work.

Notes

The authors declare no competing financial interest.

■ ACKNOWLEDGMENTS

The authors thank Grace M. Kim for her help with data analysis. Partial support of this research was provided by Dow Chemical Company. The MSC computational facilities were provided by ARO–DURIP and ONR-DURIP.

■ REFERENCES

(1) Bae, Y. H.; Okano, T.; Kim, S. W. *J. Polym. Sci. Part B: Polym. Phys.* **1990**, *28*, 923–936.

(2) Matsuo, E. S.; Tanaka, T. *J. Chem. Phys.* **1988**, *89*, 1695–1703.

(3) Ta, T.; Convertine, A. J.; Reyes, C. R.; Stayton, P. S.; Porter, T. M. *Biomacromolecules* **2010**, *11*, 1915–1920.

(4) Kawano, T.; Niidome, Y.; Mori, T.; Katayama, Y.; Niidome, T. *Bioconjugate Chem.* **2009**, *20*, 209–212.

(5) Okano, T.; Yamada, N.; Sakai, H.; Sakurai, Y. *J. Biomed. Mater. Res.* **1993**, *27*, 1243–1251.

(6) Yamada, N.; Okano, T.; Sakai, H.; Karikusa, F.; Sawasaki, Y.; Sakurai, Y. *Makromol. Chem., Rapid Commun.* **1990**, *11*, 571–576.

(7) Kitano, H.; Kondo, T.; Suzuki, H.; Ohno, K. *J. Colloid Interface Sci.* **2010**, *345*, 325–331.

(8) Kitano, H.; Kago, H.; Matsuura, K. *J. Colloid Interface Sci.* **2009**, *331*, 343–350.

(9) Li, S. K.; D'Emanuele, A. *J. Controlled Release* **2001**, *75*, 55–67.

(10) Terada, T.; Maeda, Y.; Kitano, H. *J. Phys. Chem.* **1993**, *97*, 3619–3622.

(11) Maeda, Y.; Tsukida, N.; Kitano, H.; Terada, T.; Yamanaka, J. *J. Phys. Chem.* **1993**, *97*, 13903–13906.

(12) Ohta, H.; Ando, I.; Fujishige, S.; Kubota, K. *J. Mol. Struct.* **1991**, *245*, 391–397.

(13) Ohta, H.; Ando, I.; Fujishige, S.; Kubota, K. *J. Polym. Sci. Part B: Polym. Phys.* **1991**, *29*, 963–968.

(14) Tamai, Y.; Tanaka, H.; Nakanishi, K. *Macromolecules* **1996**, *29*, 6750–6760.

(15) Tamai, Y.; Tanaka, H.; Nakanishi, K. *Macromolecules* **1996**, *29*, 6761–6769.

(16) Tamai, Y.; Tanaka, H.; Nakanishi, K. *Mol. Simul.* **1996**, *16*, 359–374.

(17) Netz, P. A.; Dorfmüller, T. *J. Chem. Phys.* **1997**, *107*, 9221–9233.

(18) Netz, P. A.; Dorfmüller, T. *J. Phys. Chem. B* **1998**, *102*, 4875–4886.

(19) Tonsing, T.; Oldiges, C. *Phys. Chem. Chem. Phys.* **2001**, *3*, 5542–5549.

(20) Longhi, G.; Lebon, F.; Abbate, S.; Fornili, S. L. *Chem. Phys. Lett.* **2004**, *386*, 123–127.

(21) Gangemi, F.; Longhi, G.; Abbate, S.; Lebon, F.; Cordone, R.; Ghilardi, G. P.; Fornili, S. L. *J. Phys. Chem. B* **2008**, *112*, 11896–11906.

(22) Deshmukh, S.; Mooney, D. A.; McDermott, T.; Kulkarni, S.; MacElroy, J. M. D. *Soft Matter* **2009**, *5*, 1514–1521.

(23) Deshmukh, S.; Mooney, D. A.; MacElroy, J. M. D. *Mol. Simul.* **2011**, *37*, 846–854.

(24) LeMieux, M. C.; Peleshanko, S.; Anderson, K. D.; Tsukruk, V. V. *Langmuir* **2007**, *23*, 265–273.

(25) Stuart, M. A. C.; Huck, W. T. S.; Genzer, J.; Muller, M.; Ober, C.; Stamm, M.; Sukhorukov, G. B.; Szleifer, I.; Tsukruk, V. V.; Urban, M.; Winnik, F.; Zauscher, S.; Luzinov, I.; Minko, S. *Nat. Mater.* **2010**, *9*, 101–113.

(26) Luzinov, I.; Minko, S.; Tsukruk, V. V. *Soft Matter* **2008**, *4*, 714–725.

(27) Yoshida, R.; Uchida, K.; Kaneko, Y.; Sakai, K.; Kikuchi, A.; Sakurai, Y.; Okano, T. *Nature* **1995**, *374*, 240–242.

(28) Kanazawa, H.; Yamamoto, K.; Matsushima, Y.; Takai, N.; Kikuchi, A.; Sakurai, Y.; Okano, T. *Anal. Chem.* **1996**, *68*, 100–105.

(29) Vidyasagar, A.; Majewski, J.; Toomey, R. *Macromolecules* **2008**, *41*, 919–924.

(30) Zhu, P. W.; Napper, D. H. *J. Chem. Phys.* **1997**, *106*, 6492–6498.

(31) Walldal, C.; Wall, S. *Colloid Polym. Sci.* **2000**, *278*, 936–945.

(32) Balamurugan, S.; Mendez, S.; Balamurugan, S. S.; O'Brien, M. J.; Lopez, G. P. *Langmuir* **2003**, *19*, 2545–2549.

(33) Yim, H.; Kent, M. S.; Huber, D. L.; Satija, S.; Majewski, J.; Smith, G. S. *Macromolecules* **2003**, *36*, 5244–5251.

(34) Yim, H.; Kent, M. S.; Mendez, S.; Balamurugan, S. S.; Balamurugan, S.; Lopez, G. P.; Satija, S. *Macromolecules* **2004**, *37*, 1994–1997.

(35) Yim, H.; Kent, M. S.; Mendez, S.; Lopez, G. P.; Satija, S.; Seo, Y. *Macromolecules* **2006**, *39*, 3420–3426.

(36) Yim, H.; Kent, M. S.; Satija, S.; Mendez, S.; Balamurugan, S. S.; Balamurugan, S.; Lopez, C. P. *J. Polym. Sci. Part B: Polym. Phys.* **2004**, *42*, 3302−3310.
(37) Yim, H.; Kent, M. S.; Satija, S.; Mendez, S.; Balamurugan, S. S.; Balamurugan, S.; Lopez, G. P. *Phys. Rev. E* **2005**, *72*.
(38) Liu, G. M.; Zhang, G. Z. *J. Phys. Chem. B* **2005**, *109*, 743−747.
(39) Annaka, M.; Yahiro, C.; Nagase, K.; Kikuchi, A.; Okano, T. *Polymer* **2007**, *48*, 5713−5720.
(40) Kidoaki, S.; Ohya, S.; Nakayama, Y.; Matsuda, T. *Langmuir* **2001**, *17*, 2402−2407.
(41) Jones, D. M.; Smith, J. R.; Huck, W. T. S.; Alexander, C. *Adv. Mater.* **2002**, *14*, 1130−1134.
(42) Plunkett, K. N.; Zhu, X.; Moore, J. S.; Leckband, D. E. *Langmuir* **2006**, *22*, 4259−4266.
(43) Zhu, X.; Yan, C.; Winnik, F. M.; Leckband, D. *Langmuir* **2007**, *23*, 162−169.
(44) Malham, I. B.; Bureau, L. *Langmuir* **2010**, *26*, 4762−4768.
(45) Tanaka, N.; Matsukawa, S.; Kurosu, H.; Ando, I. *Polymer* **1998**, *39*, 4703−4706.
(46) Takei, Y. G.; Aoki, T.; Sanui, K.; Ogata, N.; Sakurai, Y.; Okano, T. *Macromolecules* **1994**, *27*, 6163−6166.
(47) Yakushiji, T.; Sakai, K.; Kikuchi, A.; Aoyagi, T.; Sakurai, Y.; Okano, T. *Langmuir* **1998**, *14*, 4657−4662.
(48) Kobayashi, J.; Kikuchi, A.; Sakai, K.; Okano, T. *Anal. Chem.* **2001**, *73*, 2027−2033.
(49) Park, Y. S.; Ito, Y.; Imanishi, Y. *Langmuir* **1998**, *14*, 910−914.
(50) Rao, G. V. R.; Krug, M. E.; Balamurugan, S.; Xu, H. F.; Xu, Q.; Lopez, G. P. *Chem. Mater.* **2002**, *14*, 5075−5080.
(51) Chen, J. H.; Yoshida, M.; Maekawa, Y.; Tsubokawa, N. *Polymer* **2001**, *42*, 9361−9365.
(52) Abu-Lail, N. I.; Kaholek, M.; LaMattina, B.; Clark, R. L.; Zauscher, S. *Sens. Actuators, B* **2006**, *114*, 371−378.
(53) Yamato, M.; Konno, C.; Utsumi, M.; Kikuchi, A.; Okano, T. *Biomaterials* **2002**, *23*, 561−567.
(54) Akiyama, Y.; Kikuchi, A.; Yamato, M.; Okano, T. *Langmuir* **2004**, *20*, 5506−5511.
(55) Ista, L. K.; Perez-Luna, V. H.; Lopez, G. P. *Appl. Environ. Microbiol.* **1999**, *65*, 1603−1609.
(56) von Recum, H.; Okano, T.; Kim, S. W. *J. Controlled Release* **1998**, *55*, 121−130.
(57) Duracher, D.; Elaissari, A.; Mallet, F.; Pichot, C. *Langmuir* **2000**, *16*, 9002−9008.
(58) Taniguchi, T.; Duracher, D.; Delair, T.; Elaissari, A.; Pichot, C. *Colloids Surf., B* **2003**, *29*, 53−65.
(59) Ishida, N.; Biggs, S. *Macromolecules* **2010**, *43*, 7269−7276.
(60) Bae, Y. H.; Okano, T.; Kim, S. W. *Pharm. Res.* **1991**, *8*, 624−628.
(61) Bae, Y. H.; Okano, T.; Kim, S. W. *Pharm. Res.* **1991**, *8*, 531−537.
(62) Mayo, S. L.; Olafson, B. D.; Goddard, W. A. *J. Phys. Chem.* **1990**, *94*, 8897−8909.
(63) Lee, S. G.; Choi, J. I.; Koh, W.; Jang, S. S.; Kim, J.; Kim, G. *IEEE Trans. Compon., Packag., Manuf. Technol.* **2011**, *1*, 1533−1542.
(64) Lee, S. G.; Jang, S. S.; Kim, J.; Kim, G. *IEEE Trans. Adv. Packag.* **2010**, *33*, 333−339.
(65) Jang, S. S.; Lin, S. T.; Cagin, T.; Molinero, V.; Goddard, W. A. *J. Phys. Chem. B* **2005**, *109*, 10154−10167.
(66) Jang, S. S.; Molinero, V.; Cagin, T.; Goddard, W. A. *J. Phys. Chem. B* **2004**, *108*, 3149−3157.
(67) Jang, S. S.; Goddard, W. A. *J. Phys. Chem. C* **2007**, *111*, 2759−2769.
(68) Brunello, G.; Lee, S. G.; Jang, S. S.; Qi, Y. *J. Renewable Sustainable Energy* **2009**, *1*, 033101.
(69) Brunello, G. M., W. R.; Lee, S. G.; Choi, J. I.; Jang, S. S. *J. Renewable Sustainable Energy* **2011**, *3*, 043111.
(70) Jang, S. S.; Jang, Y. H.; Kim, Y. H.; Goddard, W. A.; Flood, A. H.; Laursen, B. W.; Tseng, H. R.; Stoddart, J. F.; Jeppesen, J. O.; Choi, J. W.; Steuerman, D. W.; DeIonno, E.; Heath, J. R. *J. Am. Chem. Soc.* **2005**, *127*, 1563−1575.
(71) Jang, Y. H.; Jang, S. S.; Goddard, W. A. *J. Am. Chem. Soc.* **2005**, *127*, 4959−4964.
(72) Jang, S. S.; Jang, Y. H.; Kim, Y. H.; Goddard, W. A.; Choi, J. W.; Heath, J. R.; Laursen, B. W.; Flood, A. H.; Stoddart, J. F.; Norgaard, K.; Bjornholm, T. *J. Am. Chem. Soc.* **2005**, *127*, 14804−14816.
(73) Jang, S. S.; Goddard, W. A.; Kalani, M. Y. S. *J. Phys. Chem. B* **2007**, *111*, 1729−1737.
(74) Jang, S. S.; Goddard, W. A.; Kalani, M. Y. S.; Myung, D.; Frank, C. W. *J. Phys. Chem. B* **2007**, *111*, 14440.
(75) Lee, S. G.; Brunello, G. F.; Jang, S. S.; Bucknall, D. G. *Biomaterials* **2009**, *30*, 6130−6141.
(76) Lee, S. G.; Brunello, G. F.; Jang, S. S.; Lee, J. H.; Bucknall, D. G. *J. Phys. Chem. B* **2009**, *113*, 6604−6612.
(77) Lee, S. G.; Koh, W.; Brunello, G. F.; Choi, J. I.; Bucknall, D. G.; Jang, S. S. *Theor. Chem. Acc.* **2012**, *131*, 1206.
(78) Levitt, M.; Hirshberg, M.; Sharon, R.; Laidig, K. E.; Daggett, V. *J. Phys. Chem. B* **1997**, *101*, 5051−5061.
(79) Swope, W. C.; Andersen, H. C.; Berens, P. H.; Wilson, K. R. *J. Chem. Phys.* **1982**, *76*, 637−649.
(80) Hoover, W. G. *Phys. Rev. A* **1985**, *31*, 1695−1697.
(81) Nose, S. *J. Chem. Phys.* **1984**, *81*, 511−519.
(82) Nose, S. *Mol. Phys.* **1984**, *52*, 255−268.
(83) Mulliken, R. S. *J. Chem. Phys.* **1955**, *23*, 1833−1840.
(84) Jaguar; 7.0 ed.; Schrödinger, LLC: New York, 2007.
(85) Hockney, R. W.; Eastwood, J. W. *Computer simulation using particles*; McGraw-Hill International Book Co.: New York, 1981.
(86) Plimpton, S. *J. Comput. Phys.* **1995**, *117*, 1−19.
(87) Plimpton, S. J.; Pollock, R.; Stevens, M. Particle-mesh ewald and rRESPA for parallel molecular dynamics simulations. In *The Eighth SIAM Conference on Parallel Processing for Scientific Computing* Minneapolis, MN, 1997.
(88) Lin, S. T.; Maiti, P. K.; Goddard, W. A. *J. Phys. Chem. B* **2010**, *114*, 8191−8198.
(89) Lin, S. T.; Blanco, M.; Goddard, W. A. *J. Chem. Phys.* **2003**, *119*, 11792−11805.
(90) Lin, S. T.; Maiti, P. K.; Goddard, W. A. *J. Phys. Chem. B* **2005**, *109*, 8663−8672.
(91) Li, Y. Y.; Lin, S. T.; Goddard, W. A. *J. Am. Chem. Soc.* **2004**, *126*, 1872−1885.
(92) Jang, S. S.; Lin, S. T.; Maiti, P. K.; Blanco, M.; Goddard, W. A.; Shuler, P.; Tang, Y. C. *J. Phys. Chem. B* **2004**, *108*, 12130−12140.
(93) Jana, B.; Pal, S.; Maiti, P. K.; Lin, S. T.; Hynes, J. T.; Bagchi, B. *J. Phys. Chem. B* **2006**, *110*, 19611−19618.
(94) Pascal, T. A.; He, Y.; Jiang, S.; Goddard, W. A. *J. Phys. Chem. Lett.* **2011**, *2*, 1757−1760.
(95) Pascal, T. A.; Goddard, W. A.; Jung, Y. *Proc. Natl. Acad. Sci. U.S.A.* **2011**, *108*, 11794−11798.
(96) Silberberg, A.; Eliassaf, J.; Katchalsky, A. *J. Polym. Sci.* **1957**, *23*, 259−284.
(97) Maeda, Y.; Higuchi, T.; Ikeda, I. *Langmuir* **2001**, *17*, 7535−7539.
(98) Ahmed, Z.; Gooding, E. A.; Pimenov, K. V.; Wang, L. L.; Asher, S. A. *J. Phys. Chem. B* **2009**, *113*, 4248−4256.
(99) Luzar, A.; Chandler, D. *J. Chem. Phys.* **1993**, *98*, 8160−8173.